arXiv:hep-ex/0111019 v1 6 Nov 2001

STRUCTURE OF VIRTUAL PHOTONS AT HERA *

K. SEDLÁK †
Institute of Physics, AS CR, Na Slovance 2, Praha 8, 182 21, Czech Republic
E-mail: ksedlak@fzu.cz
On behalf of the H1 and ZEUS Collaborations

Triple differential dijet cross-sections in $e^{\pm}p$ interactions measured with the H1 and ZEUS detectors at HERA are presented. The data are compared to Monte Carlo simulations which differ in their assumptions about photon structure and parton evolution. Effects of the resolved processes of longitudinally polarized virtual photons at HERA are investigated for the first time.

1 Dijet Production at HERA

The production of dijet events at HERA is dominated by processes, in which a virtual photon, radiated from the electron, interacts with a parton in the proton. In the region of photon virtuality $Q^2 \gg \Lambda^2_{QCD}$, hard collisions of the photons do not necessitate the introduction of the concept of the resolved photon (as for the real photon) and the process can in principle be described by the direct photon contribution alone, in which the photon interacts as a whole with partons from the proton.

The analyses presented here explore the region $\Lambda^2_{QCD} \ll Q^2 \lesssim E_t^2$, where different theoretical approaches can be used to take into account higher order corrections.

a) LO direct and resolved interactions based on the DGLAP evolution equations and parton showers allows the effects of transversally and also longitudinally polarized resolved photon interactions to be studied [1,2]. Since the cross section for longitudinal photons vanishes in the photoproduction regime due to gauge invariance, and the concept of a resolved photon breaks down for $Q^2 > E_t^2$, the only evidence for this phenomena can be observed in the region $0 < Q^2 \ll E_t^2$. The main difference between the longitudinal (γ_L^*) and transverse (γ_T^*) virtual photon arises from the dependence of the respective fluxes on y. While for $y \to 0$, both transverse and longitudinal fluxes are approximately same, the longitudinal flux vanishes for $y \to 1$. Also the dependence of the point-like (i.e. perturbatively calculable) part of the photon Parton Distribution Functions (PDF) on Q^2 and E_t^2 differs – while the γ_T^* PDF is proportional to $\ln(E_t^2/Q^2)$, the γ_L^* PDF depends on the scale in a

*Talk given at PHOTON 2001 Conference, Ascona, Switzerland, September 2001
†Supported by GA AVČR grant B1010005, and projects INGO-LA 116/2000, LN00A006

typically hadron-like manner.

b) k$_t$ unordered initial QCD cascades accompanying the hard process, employed for example in BFKL or CCFM evolution, can lead to final states in which the partons with the largest k_t may come from the cascade, and not, as in DGLAP evolution, from the hard subprocess. Such events may have a similar topology as is observed for the resolved interactions introduced in the previous paragraph. This possibility is investigated using the CASCADE generator [3,4] based on the CCFM evolution equation.

c) NLO calculations with and without the concept of the resolved virtual photon offer another natural possibility to be examined. Such comparisons are envisaged.

All of these three approaches include higher order corrections to the LO QCD matrix elements; however, each of the approaches treats them differently.

2 Measurement of Dijet Cross-Section

The selection criteria defining the H1 and ZEUS dijet samples are summarized in Table 1: Q^2 denotes the photon virtuality, y is the inelasticity, s is the total

H1 (16.3 pb^{-1}, 1999)	**ZEUS** (38.2 pb^{-1}, 1996-97)
$\sqrt{s} = 318$ GeV	$\sqrt{s} = 300$ GeV
$2\ \mathrm{GeV}^2 < Q^2 < 80\ \mathrm{GeV}^2$	$0.1 < Q^2 < 10\,000\ \mathrm{GeV}^2$
$0.1 < y < 0.85$	$0.2 < y < 0.55$
$E_t^{jet\,1,2} > 5$ GeV $\overline{E_t} > 6$ GeV	$E_t^{jet\,1} > 7.5$ GeV $E_t^{jet\,2} > 6.5$ GeV
$-2.5 < \eta^{jet\,1,2} < 0$	$-3 < \eta^{jet\,1,2} < 0$

Table 1. Selection criteria of the dijet samples.

electron-proton centre-of-mass energy, $E_t^{\mathrm{jet}\,1,2}$ and $\eta^{\mathrm{jet}\,1,2}$ are the transverse energy and pseudorapidity of the jet with the highest or second highest E_t, and $\overline{E_t}$ is defined as $(E_t^{\mathrm{jet}\,1} + E_t^{\mathrm{jet}\,2})/2$.

The measured data are corrected for detector effects using a bin-to-bin method (ZEUS) or Bayesian unfolding (H1). The largest source of systematic errors arises from the main calorimeter calibration uncertainty and, in the case of H1, also from a model dependence of the detector correction. The ZEUS measurement was presented in more detail at the EPS 2001 [5].

3 Results and Discussion

The corrected triple-differential dijet cross-section measured by ZEUS as a function of Q^2 , $\overline{E}_t^2$ and x_γ is shown in Fig. 1. A prediction of HERWIG with the SaS1D parameterization of the γ_T^* PDF, as well as the direct contribution of HERWIG is compared to the data. Since the overall normalization of the LO Monte Carlo simulation is to some extent uncertain, the HERWIG prediction has been normalized to the highest x_γ bin ($x_\gamma > 0.75$) in the data. The normalization is done separately for each $(Q^2, \overline{E}_t^2)$ bin.

In the region where $Q^2 > \overline{E}_t^2$, the data are well described by the direct HERWIG component only. Resolved interactions are needed if $Q^2 < \overline{E}_t^2$. However, even with the γ_T^* resolved processes included, HERWIG tends to underestimate the data in the lowest Q^2 region for $x_\gamma < 0.75$.

This fact is also demonstrated in Fig. 2 by the ratio of $\sigma(x_\gamma < 0.75)/\sigma(x_\gamma > 0.75)$. The slope of this distribution can be interpreted as a suppression of the virtual photon structure with increasing photon virtuality.

The corrected triple-differential dijet cross-section measured at H1 as a function of Q^2 , $\overline{E}_t^2$ and x_γ is shown in Fig. 3. The H1 measurement is performed in a different phase space (see Table 1) and Monte Carlo predictions are not normalized to the data.

A comparison of the H1 measurement with HERWIG leads to similar conclusions as drawn above for ZEUS. In addition, we can see that for the highest Q^2 range ($25 < Q^2 < 80$ GeV^2) and $x_\gamma < 0.75$, the HERWIG direct contribution almost describes the data in the lowest $\overline{E}_t^2$ bin, but is too low in the highest $\overline{E}_t^2$ bin. This indicates an importance of the resolved processes even at high Q^2 , once the hard scale, $\overline{E}_t^2$, is high enough.

Standard HERWIG with direct and γ_T^* resolved contributions underestimates the data. The description is improved by adding γ_L^* resolved photon interactions, which is done using a slightly modified HERWIG with the correct longitudinal photon flux and a recent γ_L^* PDF parameterization [2]. As demonstrated in Fig. 3, the γ_L^* resolved contribution is significant, and brings HERWIG closer to the measurement.

On the other hand, a simple enhancement of the PDF of the γ_T^* in the resolved contribution could lead to a similar prediction as the introduction of γ_L^*. To eliminate this ambiguity, the dijet cross-section has also been studied as a function of Q^2 , x_γ and y, which is shown in Fig. 4. HERWIG is below the data, even if the resolved γ_L^* is added. This may be due to the uncertainty of the overall normalization of the LO Monte Carlo prediction. In the region where $x_\gamma < 0.75$, the slope of the HERWIG prediction depends significantly on whether γ_L^* processes are included or not. The γ_L^* contributes significantly at low y, while it becomes very small compared to γ_T^* at high y. Unlike a pure enhancement of γ_T^* resolved processes by a constant factor, the addition of γ_L^* brings the y dependence of HERWIG much closer to the measurement.

As motivated in Section 1, the measured cross-sections in Fig. 3 are also compared to a prediction of the CASCADE MC program based on the CCFM evolution approach. This theoretical concept does not involve any information about the virtual photon structure and involves many fewer free parameters for tuning than the usual DGLAP-like MC programs. Nevertheless, CASCADE describes the data well, except for the Q^2 dependence. The Q^2 behavior, however, is related to the parameterization of the unintegrated PDFs used in the program, which are not yet constrained unambiguously.

4 Conclusions

The dijet cross-sections measured as a function of Q^2, $\overline{E}_t^2$, x_γ and Q^2, x_γ, y at H1 and ZEUS have been presented.

In the DGLAP evolution scheme, the importance of the γ_T^* resolved photon interactions is clearly demonstrated in the region where $\overline{E}_t^2 > Q^2$. Additional γ_L^* resolved photon contributions further improve the agreement of the HERWIG 5.9 prediction with the measurement.

Exploring the CCFM approach, the MC program CASCADE 1.0 gives a qualitative description of the measured differential cross-sections; however, the Q^2 dependence is not reproduced. On the other hand, the x_γ dependence in CASCADE is comparable to the sum of the direct and resolved contributions in DGLAP-like MC programs.

References

1. J. Chýla and M. Taševský, Eur. Phys. J. **C18** (2001), 723.
2. J. Chýla, Phys. Lett. **B488** (2000), 289.
3. H. Jung and G.P. Salam, Eur. Phys. J. **C19** (2001), 351-360.
4. H. Jung, "Heavy Quark production at HERA in k_t factorization supplemented with CCFM evolution", These proceedings.
5. ZEUS Collab., EPS 2001 conference: "The Q^2 and $\overline{E}_t^2$ dependence of dijet cross sections in $\gamma^* p$ interactions at HERA", paper no. 636.

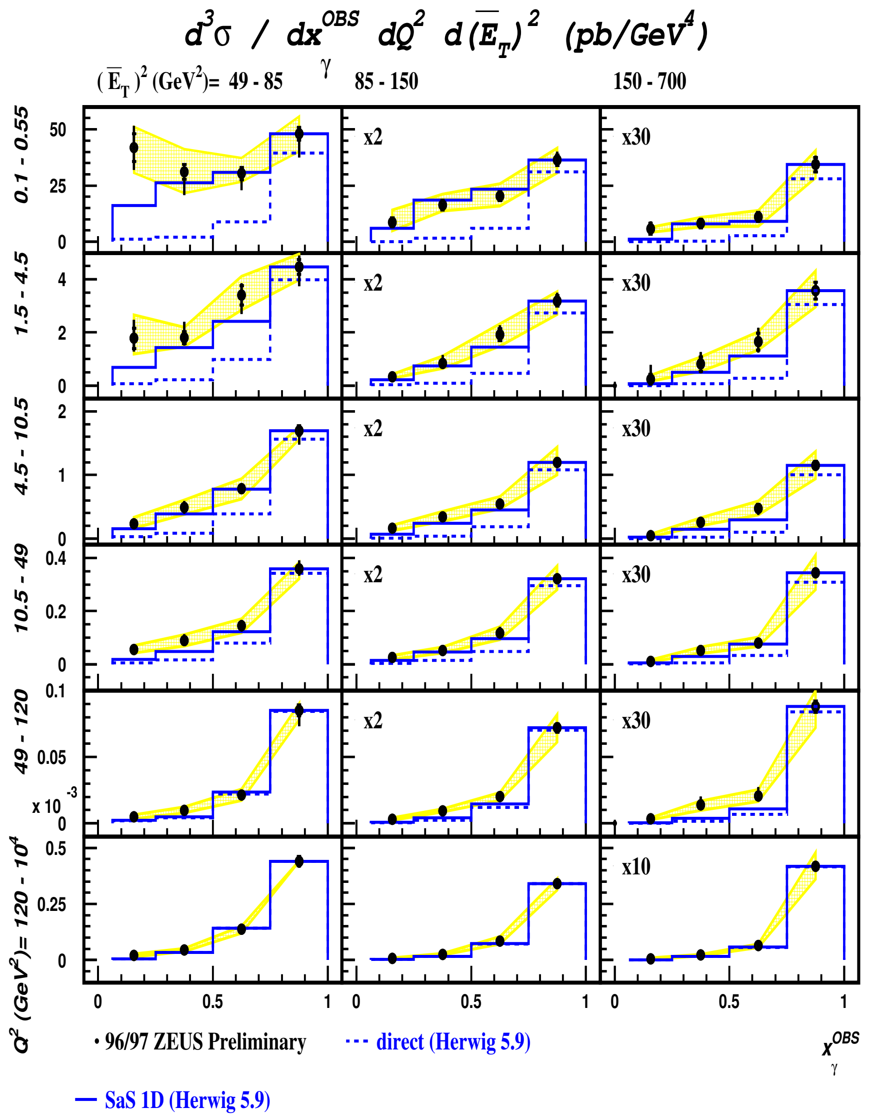

Figure 1. Triple differential dijet cross-section $d^3\sigma_{ep}/dQ^2 d\overline{E}_t^2 dx_\gamma$ for the ZEUS data is depicted by points, the shaded bands display an uncertainty estimate arising from the main calorimeter calibration. The dashed histograms represent the direct part of HERWIG only, the full line stands for the sum of the direct and transverse resolved contributions of HERWIG.

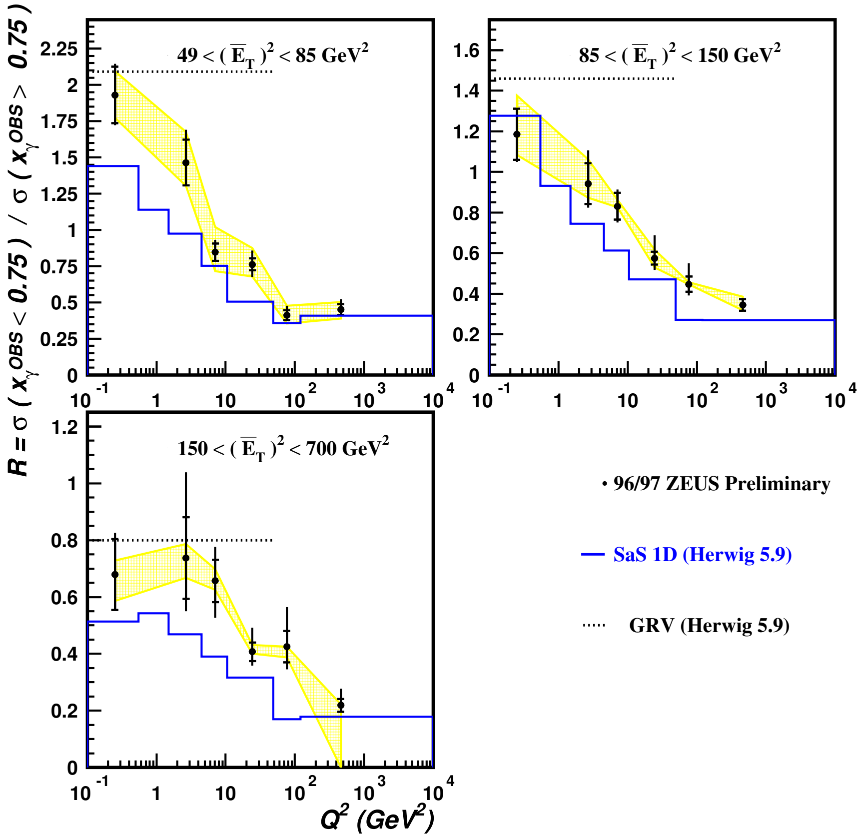

Figure 2. The ratio of cross-sections $R = \sigma(x_\gamma < 0.75)/\sigma(x_\gamma > 0.75)$ from Fig. 1.

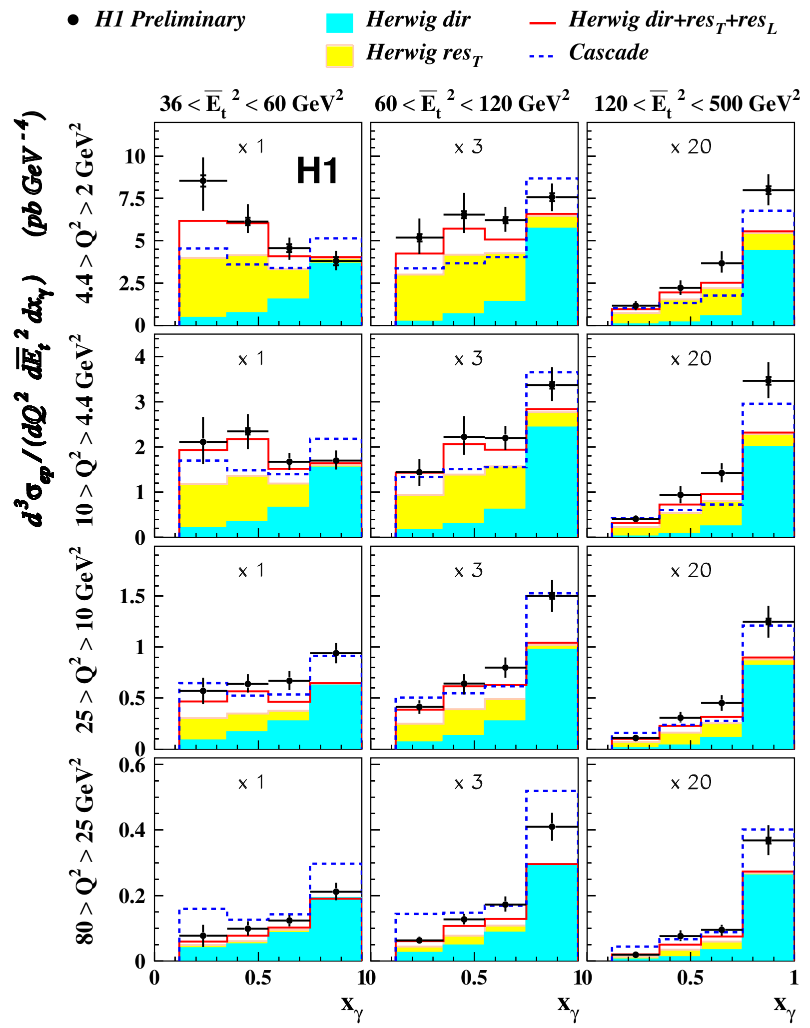

Figure 3. Triple differential dijet cross-section $d^3\sigma_{ep}/dQ^2 d\overline{E}_t^2 dx_\gamma$ for the H1 data depicted by points is compared to predictions of the HERWIG and CASCADE MC programs.

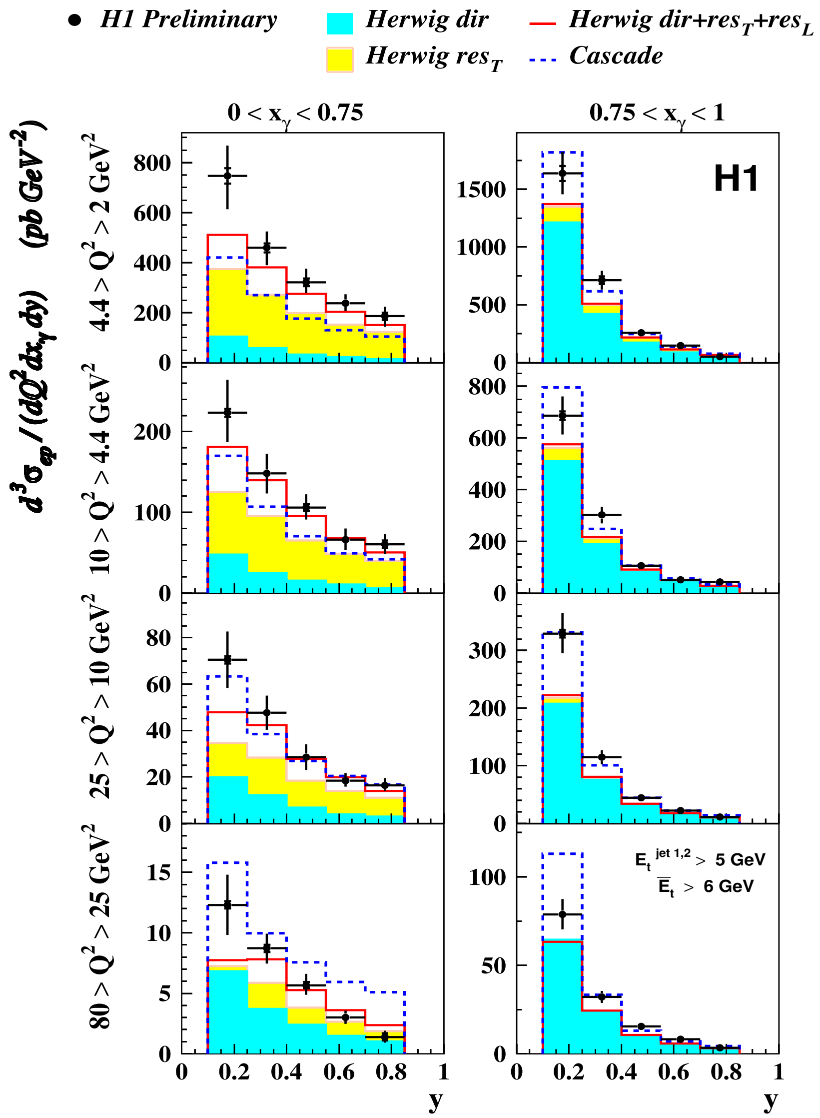

Figure 4. Triple differential dijet cross-section $d^3\sigma_{ep}/dQ^2dx_\gamma dy$.